Image Anal Stereol 2024;43:151-158 doi: 105566/ias.3021
Original Research Paper

A NEW ACTIVE CONTOUR MODEL FOR IMAGE SEGMENTATION BASED ON POTENTIAL WELL FUNCTION

XIAOTIAN WANG[1, #], ZHANG LIU[2, #], CHENCHENG HUANG[3], QI WANG[4], JIAXI WANG[1,5,✉]

[1]School of Computer Science, Chengdu University, Chengdu, China, [2]School of Biological Engineering, Wuhan Polytechnic, Wuhan, China, [3]School of Mathematics and Statistics, Chongqing Technology and Business University, Chongqing, China, [4]Department of Construction Engineering, Chengdu Aeronautic Polytechnic, Chengdu, China, [5]Key Laboratory of Pattern Recognition and Intelligent Information Processing, Institutions of Higher Education of Sichuan Province, Chengdu University, Chengdu, China

[#]The authors contributed equally
e-mail: wangxiaotian@cdu.edu.stu.cn; 562005429@qq.com; peter1234321@126.com; 540379036@qq.com; wangjiaxi@cdu.edu.cn

(Received September 7, 2023; revised May 15, 2024; accepted May 15, 2024)

ABSTRACT

In this paper, we present a modified local region-based active contour model employing an adaptive double potential well function for image segmentation. Initially, to circumvent the issue of the potential well function's excessive evolutionary pace within the zero potential well, which could lead to rapid level set evolution and inadvertent targeting of segmentation areas, we introduce an adaptive double potential well function. This function dynamically modulates coefficient by increasing the diffusion rate during the initial phase, decreasing it in the later stages, and mitigating it in the vicinity of the zero potential well. Subsequently, we incorporate a length term and a penalty term, both predicated on the adaptive double well function, into the energy functional derived from the local region-based Chan-Vese (LRCV) model. This integration serves to augment the edge smoothness of the curve and the precision of the segmentation process. Experimental outcomes demonstrate that our proposed model significantly augments segmentation accuracy when benchmarked against certain related models.

Keywords: active contour model, adaptive double potential well function, image segmentation, level set function.

INTRODUCTION

Image segmentation represents a crucial transition from image processing to image analysis, with the fundamental goal of partitioning an image into several regions of interest. In recent years, the level set method, employed for solving partial differential equations within the framework of active contour models, has emerged as a focal point of intensive research (Cheng *et al*., 2022; Xu, 2023; Shen *et al*., 2021; Gao, 2020; Zheng, 2022; Mao *et al*.,2019). And the active contour model, grounded in the level set technique, has proven to be a highly effective approach for tackling image segmentation challenges.

In 1988, Osher and Sethian introduced the level set model (Osher and Sethian, 1988), a concept grounded in fluid mechanics. This innovative model translated the complex issue of two-dimensional curve evolution into the more manageable problem of evolving three-dimensional level set function surfaces. This approach effectively resolves the challenges of curve evolution through numerical methods. Consequently, it has found widespread application in computer vision and image processing fields. In 1989, Mumford and Shah introduced the Mumford-Shah (MS) model (Mumford and Shah., 1989), establishing a fundamental framework that underpins image segmentation models. However, the reliance of the MS model on global information renders it less suitable for segmenting images characterized by intensity inhomogeneity. In 2001, Chan and Vese proposed the Chan-Vese (CV) model (Chan and Vese, 2001), a seminal active contour model rooted in the level set methodology. The CV model boasts the benefits of rapid segmentation and a reduced sensitivity to the initial contour placement; however, it often struggles with effectively segmenting images exhibiting intensity inhomogeneity. In 2008, Li and Kao introduced Region Scalable Fitting (RSF) model (Li and Kao, 2008) tailored for segmenting images with intensity inhomogeneity. This model has been extensively adopted in the domain of medical image segmentation.

However, RSF model is quite sensitive to the initial contour's positioning, and it requires four convolution operations in each iteration of the process. Consequently, the RSF model necessitates an extended segmentation duration. In 2010, Li and Xu introduced the Distance Regularized Level Set Evolution (DRLSE) model (Li *et al.*, 2010). The DRLSE model incorporates a penalty term predicated on the double potential well function, circumventing the need for periodic reinitialization of the level set function and enhancing the evolutionary pace of the level set. However, the double potential well function's evolution speed within the zero potential well peaks, causing rapid level set evolution and potentially leading to the encroachment of the zero-level set into the intended segmentation targets. As a result, the DRLSE model may fall short of delivering satisfactory segmentation outcomes (Sun *et al.*, 2013). In 2012, Liu and Peng introduced Local Region Chan-Vese (LRCV) model by leveraging the local image information (Li *et al.*, 2010). The LRCV model is capable of effectively segmenting images characterized by intensity inhomogeneity, and it performs the task at a speed slightly faster than the RSF model. However, the RSF model primarily focuses on local features and exhibits heightened sensitivity to the initial contour, which can result in a reduced level of segmentation accuracy (Zhang *et al.*, 2015).

Motivated by the aforementioned studies, we have proposed a novel LRCV model grounded in an adaptive double potential well function. Initially, we devised an adaptive double potential well function aimed at minimizing the chance of the zero-level set penetrating the interior of the target being segmented. This was achieved by enhancing the diffusion rate during the initial phase of segmentation, diminishing it in the later stages, and reducing it in proximity to the zero potential well. Subsequently, we refined the LRCV model by incorporating a length term (Chan and Vese, 2001) and a penalty term based on the adaptive double potential well function into the energy functional. This modification serves to enhance the smoothness of the curve edge and elevate the precision of segmentation.

The remainder of this paper is structured as follows: In Section 2, we provide a concise review of the LRCV model and the DRLSE model. In Section 3, we introduce the modified model. In Section 4, we detail the numerical algorithms and present the experimental outcomes. Finally, in Section 5, we offer a summary of our paper.

BACKGROUND

The LRCV model

To more effectively segment images exhibiting intensity inhomogeneity, Liu developed the LRCV model, which is an evolution of the CV model. The energy functional for the LRCV model is defined as follows:

$$E\left(c_1(x), c_2(x), \varphi(x)\right) = \sum_{i=1}^{2} \lambda_i \int_{\Omega} \left|I(x) - c_i(x)\right|^2 M_i\left(\varphi(x)\right) dx \tag{1}$$

where φ is the level set function, I is the input image, λ_i is the weight coefficient of each energy term, $c_i(x)$ represent the local gray mean of the internal and external images of the evolution curve, M_i is defined as follows:

$$M_i(\varphi) = \begin{cases} H_\varepsilon(\varphi) & , i = 1 \\ 1 - H_\varepsilon(\varphi) & , i = 2 \end{cases} \tag{2}$$

where H_ε is Heaviside function, ε is normal number. The evolution equation of level set of Equation (1) can be obtained by using gradient flows method (Wang D K, 2008):

$$\frac{\partial \varphi}{\partial t} = \delta_\varepsilon(\varphi) \cdot \left[-\lambda_1\left(I(x) - c_1(x)\right)^2 + \lambda_2\left(I(x) - c_2(x)\right)^2\right] \tag{3}$$

where δ_ε is Dirac function. The LRCV model demonstrates effective performance in segmenting images with intensity inhomogeneity by utilizing local image information. However, the LRCV model's reliance solely on local features makes it more sensitive to the initial contour, consequently diminishing segmentation accuracy.

The LRCV model

To circumvent the decreased efficiency resulting from the periodic reinitialization of the level set function, Li incorporated a penalty term based on the double potential well function and introduced the DRLSE model. The energy functional of the DRLSE model is defined as follows:

$$\begin{aligned} E\left(\varphi(x)\right) = {} & \lambda \int_{\Omega} g(x)\, \delta_\varepsilon\left(\varphi(x)\right) \left|\nabla \varphi\right| dx \\ & + \nu \int_{\Omega} g(x)\, H_\varepsilon\left(-\varphi(x)\right) dx \\ & + \mu \int_{\Omega} p\left(\left|\nabla \varphi\right|\right) dx \end{aligned} \tag{4}$$

where g is the edge stop function, p is the double potential well function, which is used to maintain the sign distance characteristic of the level set function $|\nabla \varphi| = 1$, and p is defined as follows:

$$p(s) = \begin{cases} \frac{1}{(2\pi)^2}\left(1-\cos(2\pi s)\right), s \le 1 \\ \frac{1}{2}(s-1)^2 \qquad\qquad , s > 1 \end{cases} \tag{5}$$

where s is expressed as $|\nabla\varphi|$. The evolution equation of level set of Equation (4) can be obtained by using gradient flows method:

$$\frac{\partial\varphi}{\partial t} = \lambda\delta_\varepsilon(\varphi)\,div\left(g\frac{\nabla\varphi}{|\nabla\varphi|}\right) + \nu g\delta_\varepsilon(\varphi) + \mu div\left(d_p\left(|\nabla\varphi|\right)\nabla\varphi\right) \tag{6}$$

where d is the double potential well diffusion rate function, which is defined as follows:

$$d_p(s) = \frac{p'(s)}{s} = \begin{cases} \frac{\sin(2\pi s)}{2\pi s}, s \le 1 \\ 1-\frac{1}{s} \qquad , s > 1 \end{cases} \tag{7}$$

Equation (7) is illustrated by Fig. 1. The double potential well diffusion rate function reaches its maximum evolution speed in the vicinity of the zero potential well, enabling rapid advancement of the level set, which can inadvertently cause the level set to penetrate the interior of the segmentation target. Consequently, this may result in suboptimal segmentation outcomes with the DRLSE model.

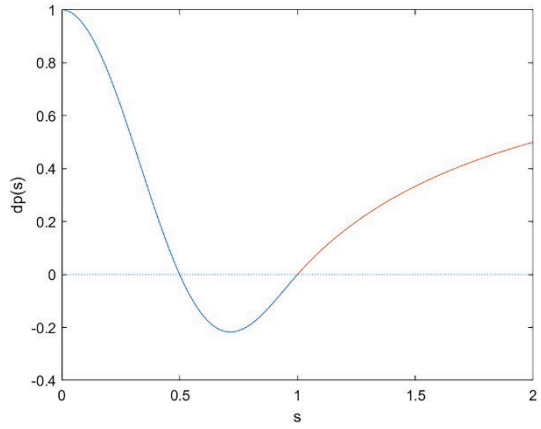

Fig. 1. *Double well diffusion rate function of DRLSE model.*

Modified model

In order to enhance the segmentation accuracy, we have devised an adaptive double potential well function and introduced an innovative local region-based active contour model. This new model incorporates an additional length term and a penalty term into the energy functional of the LRCV model. The length term contributes to the smoothness and continuity of the curve's edge, while the penalty term preserves the signed distance property of the level set function $|\nabla\varphi| = 1$. Moreover, to prevent the potential well function from evolving excessively swiftly in the zero potential wells, we devised an adaptive double potential well function to serve as the penalty term. The operating principle of the adaptive double well function is structured as follows: Initially, the diffusion rate function is segmented into three distinct sections. We then substituted a function characterized by a transverse intercept of 0.5 and a diminished vertical intercept, which served to decrease the rate of diffusion proximal to the zero potential well within the specified interval $s \in [0,0.5]$. Finally, we introduced an adaptive coefficient to the function, enabling the diffusion rate to gradually increase during the initial stages of evolution, and subsequently decrease in the later stages. Such strategies enhance the utilization of global information, leading to more precise segmentation results.

The adaptive double well function and diffusion rate function proposed in this paper are defined as follows:

$$q(s) = \begin{cases} k(i)\frac{s^2(1-2s^2)}{5} , 0 \le s \le 0.5 \\ k(i)\frac{(1-\cos(2\pi s))}{80} , 0.5 < s \le 1 \\ k(i)\frac{(s-1)^2}{2} \qquad , s > 1 \end{cases} \tag{8}$$

$$d_q(s) = \begin{cases} k(i)\frac{2(1-4s^2)}{5} , 0 \le s \le 0.5 \\ k(i)\frac{\pi\sin(2\pi s)}{40s} , 0.5 < s \le 1 \\ k(i)\frac{s-1}{s} \qquad , s > 1 \end{cases} \tag{9}$$

where $|\nabla\varphi|$ is represented as s, and $k(i)$ is the adaptive coefficient, which is defined as follows:

$$k(i) = \alpha\left[1+\sin\left(\frac{3\pi\cdot i}{2\cdot i_{max}}\right)\right] \tag{10}$$

where α is the diffusion coefficient which controls the variation range of diffusion rate. i is the current iteration number, i_{max} is the maximum iteration number. When $\alpha = 1$, $i = 0$, Equation (9) is illustrated in Fig. 2. Observations from Fig. 2 reveal a significant reduction in the diffusion rate proximal to the zero potential well. When $s > 1$, the diffusion rate is positive and the level set is forward diffusion, which makes s reduce to 1. When $0.5 < s < 1$, the diffusion rate is negative and the level set is backward diffusion, which makes s increase

to 1; When $s < 0.5$, the diffusion rate is positive and the level set is forward diffusion, which makes s reduce to 0. The introduction of the adaptive coefficient allows for the diffusion function to dynamically expand and contract vertically as iterations progress.

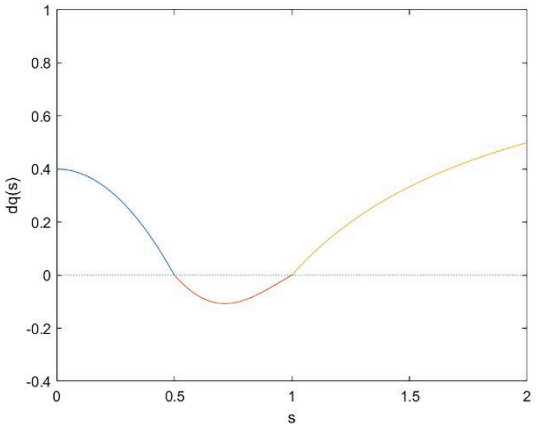

Fig. 2: *Adaptive double well diffusion rate function.*

By adding the length term and the penalty term into the energy functional of the LRCV model, the energy functional in this paper can be obtained as follows:

$$\begin{aligned} &E\left(c_1(x), c_2(x), \varphi(x)\right) = \\ &\sum_{i=1}^{2} \lambda_i \int_{\Omega} \left|I(x) - c_i(x)\right|^2 M_i\left(\varphi(x)\right) dx + \\ &\nu \int_{\Omega} \delta_{\varepsilon}\left(\varphi(x)\right) \left|\nabla\varphi\right| dx + \mu \int_{\Omega} q\left(\left|\nabla\varphi\right|\right) dx \end{aligned} \tag{11}$$

where φ is the level set function, I is the input image, $\lambda_1, \lambda_2, \nu$ and μ are the weight coefficient of each energy term, $c_1(x)$ and $c_2(x)$ represent the local gray mean of the internal and external images of the evolution curve respectively, δ_{ε} is the Dirac function, ε is the normal number, q is the adaptive double potential well function, M_i defined as follows:

$$M_i(\varphi) = \begin{cases} H_{\varepsilon}(\varphi) & , i = 1 \\ 1 - H_{\varepsilon}(\varphi), & i = 2 \end{cases} \tag{12}$$

where H_{ε} is the Heaviside function, ε is a normal number, $c_1(x)$ and $c_2(x)$ are defined as follows:

$$\begin{cases} c_1(x) = \dfrac{\int_{\Omega} g_k(x-y)\left(I(y) H_{\varepsilon}(\varphi(x))\right) dy}{\int_{\Omega} g_k(x-y) H_{\varepsilon}(\varphi(x)) dy} \\ c_2(x) = \dfrac{\int_{\Omega} g_k(x-y)\left(I(y)\left(1 - H_{\varepsilon}(\varphi(x))\right)\right) dy}{\int_{\Omega} g_k(x-y)\left(1 - H_{\varepsilon}(\varphi(x))\right) dy} \end{cases} \tag{13}$$

where g_k is the Gaussian kernel function with standard deviation is represented k.

To perform image segmentation using the level set method, it is necessary to minimize equations (11), (12), and (13). Additionally, a non-compact, smooth, and strictly monotone approximation of the Heaviside and Dirac functions is required. The approximating functions for these are as follows:

$$\begin{cases} H_{\varepsilon}(x) = \dfrac{1}{2}\left[1 + \dfrac{2}{\pi} \operatorname{arctan}\left(\dfrac{x}{\varepsilon}\right)\right] \\ \delta_{\varepsilon}(x) = H_{\varepsilon}'(x) = \dfrac{1}{\pi} \dfrac{\varepsilon}{\varepsilon^2 + x^2} \end{cases} \tag{14}$$

where ε is usually taken 1. Evolution equation of the level set can be obtained by using the gradient flows method:

$$\begin{aligned} &\frac{\partial\varphi}{\partial t} = \delta_{\varepsilon}(\varphi) \cdot \\ &\left[-\lambda_1\left(I(x) - c_1(x)\right)^2 + \lambda_2\left(I(x) - c_2(x)\right)^2\right] \\ &+\nu\delta_{\varepsilon}(\varphi)\, div\left(\frac{\nabla\varphi}{|\nabla\varphi|}\right) + \mu\, div\left(d_q\left(|\nabla\varphi|\right)\nabla\varphi\right) \end{aligned} \tag{15}$$

where $div(\cdot)$ is the divergence operator, d is an adaptive double-well diffusion rate function. Since it is challenging to derive the analytical solution of the nonlinear partial differential equation, an approximate solution is obtained through numerical computation. Finite difference method (Ames W F, 2014; Ma R, 2021) was adopted to discrete the level set function into a difference scheme, and the right end of the equation (15) was denoted as $F(\varphi)$. Finally, the iteration formula could be written as:

$$\varphi_{n+1} = \varphi_n + \Delta t \cdot F\left(\varphi_n\right) \tag{16}$$

where n is the number of iterations, Δt is the time step.

Experiments and analysis

Experiments conducted with both real and synthetic images demonstrate the high segmentation accuracy achieved by the proposed model. The experimental environment is Matlab R2019a, the hardware environment is Inter Core i5-8265U processor, 1.60GHz main frequency, 8.0G memory. This paper gives a set of reference parameters: scale parameter is $\sigma = 3$ and $\varepsilon = 1$, time step is $\Delta t = 0.1$, energy weight of LRCV is $\lambda_1 = \lambda_2 = 0.01$, and energy weight of other models is $\mu = \lambda_1 = \lambda_2 = 1$. In this paper, speed is measured by the number of iterations, and accuracy is measured by Dice Similarity Coefficient (DSC) coefficient and Relative Volume Difference (RVD) coefficient (Litjens G *et al.*, 2014). DSC is defined as follows:

$$k_{DSC} = \frac{2|x \cap y|}{|x| + |y|} \tag{17}$$

where $|x|$ and $|y|$ respectively represent the area obtained by model and ground truth. The area is represented by the number of pixels, and the distribution range is $k_{DSC} \in [0,1]$, 0 means that the two data sets have no intersection; 1 means that the two data sets are the same. RVD is defined as

$$k_{RVD} = \left(\frac{|x|}{|y|} - 1 \right) \cdot 100\% \tag{18}$$

where $|x|$ and $|y|$ are the same as in Equation (17). The smaller $|k_{RVD}|$ is, the better the segmentation effect is.

In this paper, we enhance the energy functional of the LRCV model by incorporating a length term and a penalty term based on the Double Well Function (DWF), resulting in the LRCV+DWF model. Fig. 3 shows the segmentation results of vascular images by different models. (a) represents the given initial contour, (b) represents the segmentation results of LRCV model, (c) represents the segmentation results of LRCV+DWF model, and (d) represents the segmentation results of LRCV+ADWF model. As observed in Fig. 3, the low contrast characteristic of vascular images leads the LRCV model to only partially segment the edges of the vessels. However, by incorporating length and penalty terms into the energy functionals of both the LRCV+DWF and LRCV+ADWF models, the vessel edges can be segmented more effectively.

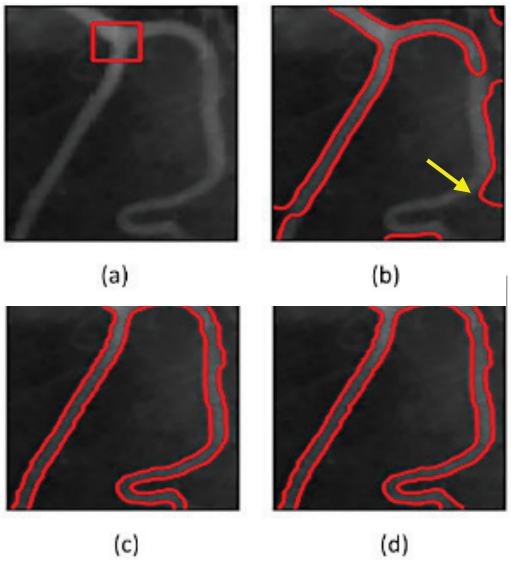

Fig. 3. *Segmentation results of different models on vascular images. (a) the initial contour, (b) the segmentation results of LRCV model, (c) the segmentation results of LRCV+DWF model, (d) the segmentation results of LRCV+ADWF model.*

Fig. 4 shows the segmentation results of manhole cover images by different models. (a) represents the given initial contour, (b) represents the segmentation results of LRCV model, (c) represents the segmentation results of LRCV+DWF model, and (d) represents the segmentation results of LRCV+ADWF model. Fig. 4 illustrates that the LRCV model suffers from over-segmentation due to the interference caused by the fringe at the bottom of the image. On the other hand, the inclusion of length and penalty terms in the energy functionals of both the LRCV+DWF and LRCV+ADWF models enables the clear and accurate segmentation of the manhole cover's edge.

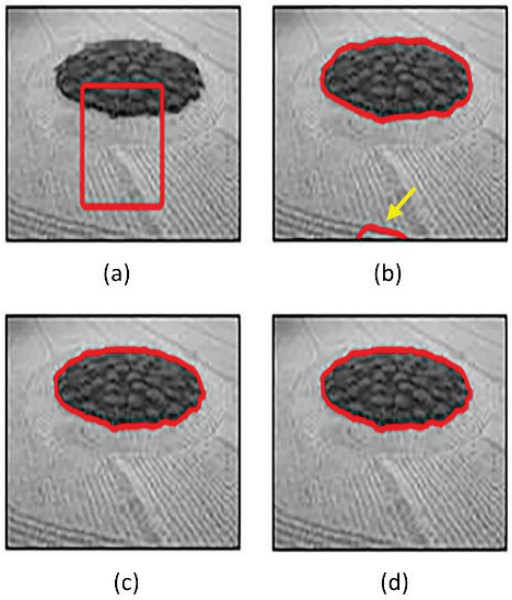

Fig. 4. *Segmentation results of different models on well cover images. (a) the initial contour, (b) the segmentation results of LRCV model, (c) the segmentation results of LRCV+DWF model, (d) the segmentation results of LRCV+ADWF model.*

Fig. 5 shows the segmentation results of simulation images by different models. (a) represents the given initial contour, (b) represents the segmentation results of LRCV model, (c) represents the segmentation results of LRCV+DWF model, and (d) represents the segmentation results of LRCV+ADWF model. As depicted in Fig. 5, the intensity inhomogeneity present in the simulated image leads the LRCV model to segment only a portion of the contour, consequently resulting in under-segmentation. The segmentation result of the LRCV+DWF model shows four red dots, which are primarily due to the zero level set penetrating into the interior of the target being segmented. Conversely, the LRCV+ADWF model employs a penalty term based on an adaptive double potential well function, allowing for a more precise and accurate segmentation of the simulation image's contour.

Fig. 6 shows the segmentation results of spider images by different models. (a) represents the given initial contour, (b) represents the segmentation results of LRCV model, (c) represents the segmentation results of LRCV+DWF model, and (d) represents the segmentation results of LRCV+ADWF model. As shown in Fig. 6, the segmentation result of the LRCV model is adversely affected by the white spots on the spider's surface, leading to a poor segmentation effect. The LRCV+ADWF model, which incorporates a penalty term based on the adaptive double potential well function, yields a superior segmentation outcome compared to the LRCV+DWF model.

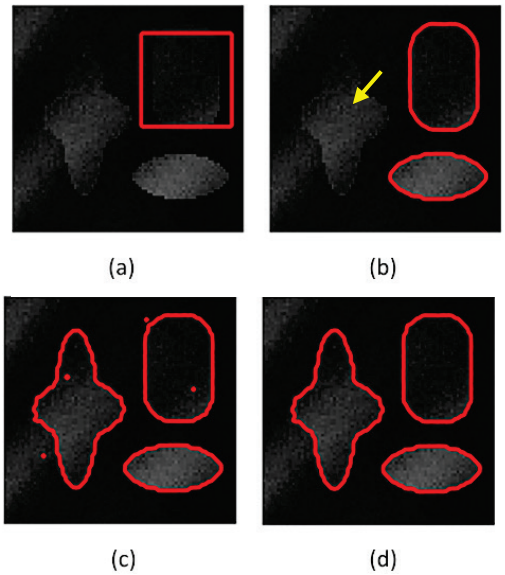

Fig. 5. *Segmentation results of different models on simulation images. (a) the initial contour, (b) the segmentation results of LRCV model, (c) the segmentation results of LRCV+DWF model, and (d) the segmentation results of LRCV+ADWF model.*

Table 1. *Comparison of iterations by three models.*

	LRCV	LRCV+DWF	LRCV+ADWF
Fig. 3	**500**	700	**500**
Fig. 4	800	700	**700**
Fig. 5	900	600	**400**
Fig. 6	700	700	**600**

Table. 1 compares the iterations of the three models. Table 1 illustrates that the LRCV+ADWF model requires fewer iterations and converges more quickly, largely due to the proposed adaptive coefficient which enables the model to achieve faster completion of segmentation. Table. 2 shows the comparison of DSC and RVD by the three models. As shown in Table 2, the LRCV+ADWF model exhibits a higher Dice Similarity Coefficient (DSC) and a lower absolute value of the Relative Volume Difference (RVD), indicating that the segmentation accuracy of the proposed model surpasses that of both the LRCV model and the LRCV+DWF model. This improvement is attributed to the adaptive double potential well function, which mitigates the chance of the zero level set penetrating into the interior of the target being segmented by reducing the diffusion rate near the zero potential well, thereby enhancing segmentation accuracy.

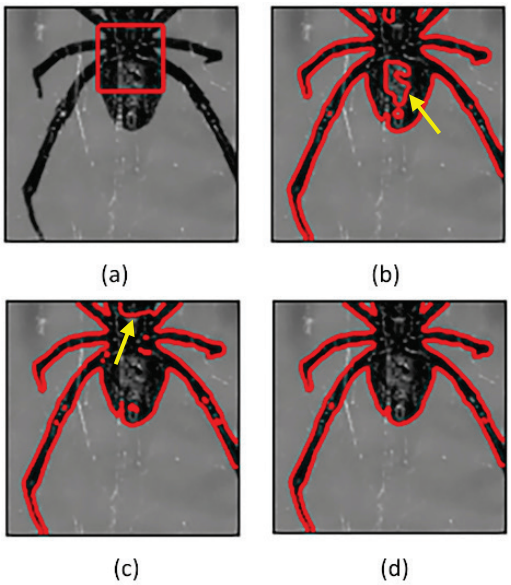

Figure. 6. *Segmentation results of different models on spider images. (a) the initial contour, (b) the segmentation results of LRCV model, (c)the segmentation results of LRCV+DWF model, (d) the segmentation results of LRCV+ADWF model.*

Table 2. *Comparison of DSC and RVD coefficients by three models*

	DSC			RVD(%)		
	LRCV	LRCV +DWF	LRCV+ ADWF	LRCV	LRCV+ DWF	LRCV+ ADWF
Fig. 3	0.5803	0.9212	**0.9258**	-19.43	-11.84	**-10.96**
Fig. 4	0.9517	0.9914	**0.9918**	6.17	-1.32	**-1.26**
Fig. 5	0.7229	0.9781	**0.9791**	-43.40	-4.00	**-4.00**
Fig. 6	0.8948	0.9067	**0.9305**	-18.75	-16.54	**-12.52**

The robustness of the proposed model is finally verified by introducing salt-and-pepper noise into the images. To ensure consistency in the noise placement across the images and to preclude any accidental errors, random seeds are deliberately set. The segmentation outcomes are displayed in Fig. 7 and Table 3, which demonstrate that the proposed algorithm exhibits superior noise resistance compared to the other two algorithms.

Table 3. *Quantitative analysis of noise experiment*

	LRCV	LRCV+DWF	LRCV+ADWF
DSC	0.5811	0.9027	**0.9244**
RVD	-19.27	-11.01	**-6.63**

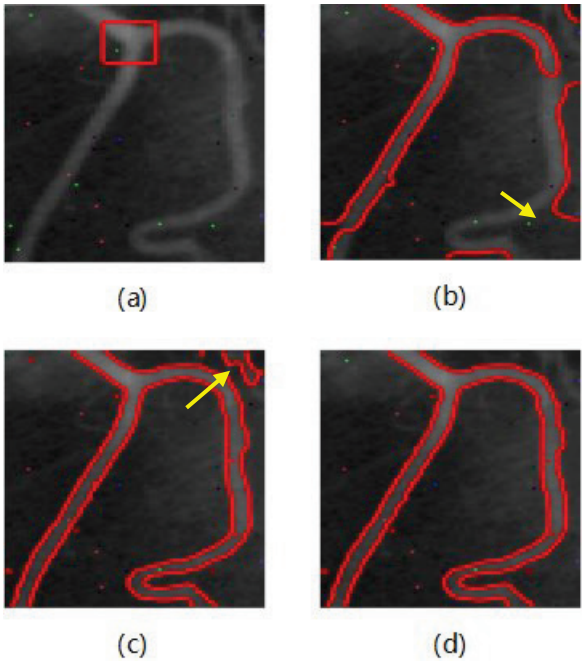

Fig. 7. *Segmentation results of different models on noisy images. (a) represents the initial contour, (b) represents the segmentation results of LRCV model, (c) represents the segmentation results of LRCV+DWF model, and (d) represents the segmentation results of LRCV+ADWF model.*

DISCUSSION

The algorithm proposed in this paper contains a large number of parameters, which will require some time to adjust.

And the task of parameter selection for a model is challenging due to various factors, such as the characteristics of the object being segmented, the model itself, and the data available. The choice of parameters is crucial for achieving better results. In general, when the model has only one parameter, the L-curve method (Yang *et al.*, 2015) can be utilized to determine the optimal value. However, when the model contains two or more parameters, they are often chosen through a process of trial and error (Zhang *et al.*, 2018). Therefore, a more thorough investigation into parameter selection strategies is necessary. Several approaches could aid in this process, including adaptive parameter selection and deep learning (Wu *et al.*, 2021; Pan, 2024), which are the focus of our future research directions.

CONCLUSION

To more effectively segment images characterized by intensity inhomogeneity, a novel local region-based active contour model is introduced. This model is founded on an adaptive double potential well function to enhance image segmentation performance. An adaptive double well function, serving as a penalty term, is proposed to dynamically adjust the coefficient and decrease the diffusion rate in the vicinity of the zero potential well. The inclusion of the length term enhances the smoothness of the curve edge. Ultimately, the integration of both the length term and the penalty term into the energy functional of the LRCV model leads to an enhancement in segmentation accuracy. Experimental results indicate that both the accuracy and the speed of the proposed model surpass those of the LRCV model and the LRCV+DWF model.

ACKNOWLEDGMENTS

This work is supported by the Chengdu University Pattern Recognition and Intelligent Information Processing Sichuan University Key Laboratory open fund (MSSB-2023), the Foundation of Guangdong Provincial Key Laboratory of Sensor Technology and Biomedical Instrument (2020B121206 0077).

REFERENCES

Ames WF (2014). Numerical methods for partial differential equations. Academic press:15-19.

Chan T, Vese L (2001). Active contours without edges. IEEE Trans Image Process 10 (2): 266-77.

Cheng YZ, Zhong LH, He X (2022). Segmentation of wood cross section pipe holes based on improved K-Means clustering and Level set. Forest Engineering, 38 (01): 42-51.

Deng LN (2019). Improvement of CV model and its application in image segmentation [D]. Xi'an University of Science and Technology.

Gao MY (2020). Research on image segmentation based on CV Level set [D]. Southwest University.

Li CM, Xu CY, Gui CF, Fox MD (2005). Level set evolution without re-initialization: a new variational formulation. 2005 IEEE Computer Society Conference on Computer Vision and Pattern Recognition (CVPR'05) 1:430-6.

Li C, Kao CY, Gore JC, Ding Z (2008). Minimization of region-scalable fitting energy for image segmentation. IEEE Transactions On Image Processing 17 (10): 1940-49.

Li CM, Xu CY, Gui CF, Fox MD (2010). Distance regularized level set evolution and its application to image

segmentation. IEEE Transactions On Image Processing 19 (12): 3243-54.

Litjens G, Toth R, van de Ven W, Hoeks C, Kerkstra S, van Ginneken B, Vincent G, Guillard G, Birbeck N, Zhang J, Strand R, Malmberg F, Ou Y, Davatzikos C, Kirschner M, Jung F, Yuan J, Qiu W, Gao Q, Edwards PE, Maan B, van der Heijden F, Ghose S, Mitra J, Dowling J, Barratt D, Huisman H, Madabhushi A (2014). Evaluation of prostate segmentation algorithms for MRI: The PROMISE12 challenge. Medical Image Analysis, 18 (2): 359-73.

Liu SG, Peng YL (2012). A local region-based Chan-Vese model for image segmentation. Pattern Recognition 45 (7): 2769-79.

Ma R (2021). Research on image segmentation method based on partial differential equation [D]. Xinjiang Normal University.

Mao L, Zhao L Q, Yu MA, Wei Y, Wang Y (2019). Parathyroid segmentation based on hybrid level set model based on image local entropy. Acta Optica Sinica 39 (12): 256-64.

Mumford DB, Shah J (1989). Optimal approximations by piecewise smooth functions and associated variational problems. Communications On Pure and Applied Mathematics 42 (5): 577-685.

Osher S, Sethian JA (1988). Fronts propagating with curvature-dependent speed: Algorithms based on Hamilton-Jacobi formulations. J Comput Phys 79 (1): 12-49.

Pan JY (2024). Iterative Residual Optimization Network for Limited-angle Tomographic Reconstruction. IEEE Transactions on Image Processing 33: 910-25

Shen YJ, Wang XP, Zhou YZ Zhang ZR (2021). Local level set mask optimization based on semi implicit discretization. Acta Optica Sinica 41 (09): 96-103.

Sun C, Xu Y L, Bi DY (2013). Distance normalized level set algorithm using V-well function. Computer Application And Software 30(4):271-274.

Wang DK, Hou YQ, Peng JY (2008). Partial differential equation method for image processing. Beijing: Science Press:103-107.

Wu WW, Hu D, Niu C, Yu H, Vardhanabhuti V, Wang G (2021). DRONE: Dual-domain residual-based optimization network for sparse-view CT reconstruction. IEEE Transactions on Medical Imaging 40 (11): 3002-3014.

Xu Z (2023). Image segmentation method based on local region and Level set regularization. Journal of Tonghua Normal University 44 (02): 28-32.

Yang X, Hofmann R, Dapp R, Kamp T, Rolo T, Xiao X, Moosmann J, Kashef J, and Stotzka R (2015). TV-based conjugate gradient method and discrete L-curve for few-view CT reconstruction of X-ray in vivo data. Optics Express 23 (5): 5368-5387.

Zhang HY, Gao SB, Zhou JB (2015). A novel active contour model method. Microelectronics and computer 32 (09): 161-163.

Zhang Y, Yang K, Zhu Y (2018). NOWNUNM: Nonlocal Weighted Nuclear Norm Minimization for Sparse-Sampling CT Reconstruction. IEEE Access 6: 73370-73379.

Zheng YR (2022). An image segmentation method based on hesitant wisdom set and Level set. Journal of Chongqing Technology and Business University (Natural Science Edition) 39 (05): 17-23.